



Chromium desalination using novel chitosan functionalized iron oxide- biochar composites: Analysis, synthesis, characterization and adsorption performance

Anurag Choudhary^{a,*} and Sardar Singh Poonia^b

^aAssistant Professor, Department of Chemistry, JNV University, Jodhpur (India)

^bResearch Scholar, Department of Chemistry, JNV University, Jodhpur (India)

ARTICLE INFO:

Received 9 Oct 2023

Revised form 12 Dec 2023

Accepted 17 Jan 2024

Available online 29 March 2024

Keywords:

Adsorption,
 Chitosan,
 Chromium,
 Spectrophotometer,
 Water Treatment

ABSTRACT

In the study, chitosan functionalized iron oxide incorporated with peanut shell biomass was prepared for potential adsorption of chromium (VI) from an aqueous media. The prepared material was characterized by modern spectroscopic methods for confirming the successful embedding. The adsorption experiments were conducted in batch systems. The experimental data showed robust removal of chromium supported by kinetic and equilibrium studies. The sorption data exhibited a strong agreement with the pseudo-second-order kinetics model, further confirming conformity with the Langmuir isotherm model. Adsorption studies were taken to find the effects of pH and time, reusability, ionic strength and presence of coexisting ions. The maximum sorption capacity was achieved as 14.28 mg g^{-1} at pH 4 and the optimum contact time was 40 minutes. The background electrolytes have much less effect on uptake efficiency and this green adsorbent can be utilized for up to four cycles. Additionally, a systematic approach was employed to ensure the precision and accuracy of the spectroscopic method. Calibration was linear in the range from 0.5 to $6.0 \mu\text{g L}^{-1}$ ($R^2 > 0.99$). The limits of detection (LOD) and quantification (LOQ) were $0.65 \mu\text{g L}^{-1}$ and $2.16 \mu\text{g L}^{-1}$, respectively. The relative standard deviation (RSD) was 7.62% ($n=7$). The method accuracy was verified by analyzing recovery ($92.8 \pm 0.5\%$ to $103.09 \pm 0.5 \%$) studies on water samples. In conclusion, novel chitosan functionalized Iron oxide-biochar composites find unbeatable, recyclable and highly efficient adsorption properties for chromium desalination.

1. Introduction

Chromium, a versatile and widely used metal, has found its way into various industrial processes, from steel production to electroplating. However, industrial waste often contains chromium heavy metal ions as a byproduct of these activities. These ions, primarily in the form of hexavalent chromium (Cr (VI)), pose significant toxicity to aquatic life and are harmful to human health. Understanding the sources, characteristics, and

potential hazards of chromium heavy metal ions from industrial waste is crucial for effectively managing and remedying these pollutants. Effective disposal of chromium from wastewater is essential to protect the environment, and human health, and ensure compliance with global regulations while promoting sustainable water management. Ecological elimination [1], chemical precipitation [2], redox [3] and adsorption [4] are only some of the methods that have been used for Cr (VI) removal so far. Adsorption is considered the best and most widely used approach for eliminating toxic contaminants due to its inexpensive, effortless, and highly influential capability. Experiments have

*Corresponding Author: Anurag Choudhary

Email: anurag051981@gmail.com

<https://doi.org/10.24200/amecj.v6.i04.281>

used a wide range of adsorbing materials, including biochar, chitosan, and iron oxide, to remove Cr (VI). The peanut (*Arachis hypogaea L.*) is an ancient crop that is widely cultivated in tropical and subtropical climates. India holds the position of being the second-largest producer of peanuts globally, following China. Peanut shells are the remainder of the initial processing of peanuts [5]. The peanut shell is a substantial byproduct of the peanut industries, constituting around 25% to 30% of the legume's total weight. These shells are discarded as such as waste after the removal of groundnut seed from its pod at the last phase of peanut processing. These are the abundant agro-industrial waste product which has a very slow degradation rate under natural conditions [6]. The peanut shell is a lignocellulosic material mainly composed of cellulose (44.8%), hemicelluloses (5.8%), and lignin (36.1%), which are complex organic polymers. To successfully manage and control this extremely troublesome detrimental species, it may be unique and enticing to convert shells into biochar and utilize them in eliminating cationic toxicants. Biochar produced from waste biomass finds varied applications in diversified realms. In agriculture, it stimulates soil fertility, water retention, and nutrient efficiency. As a stable carbon sink, biochar contributes to climate change mitigation by sequestering carbon in the soil for many years. It also acts as a water filtration medium, removing contaminants from wastewater. Its adsorption properties make it useful for environmental remediation efforts, and it can even be used as a renewable energy source [7]. Additionally, recent research has shown that biochar may be utilized as a thrifty sorbent to remove a variety of toxins from water. The biochar possesses several desirable characteristics, including a substantial specific surface area, a porous structure, an abundance of surface functional groups, and mineral components. These properties render biochar a suitable adsorbent for the removal of pollutants from aqueous solutions. Enhancements and treatment methods applied to biochar customization result in improved adsorption capabilities compared to its pristine form. By modifying, its surface properties can be tailored to target specific contaminants, making it even more effective for adsorption purposes. Consequently, a range of techniques, including chemical functionalization, physical activation, impregnation, coating, and surface oxidation, have been employed to enhance the efficacy of these materials in the context of environmental remediation [8]. Chitosan, a biopolymer derived from chitin, has gained

remarkable attention and intensively studied for its potential application in heavy metal removal due to its unique properties such as non-toxic nature, abundant, remarkable adsorption capacity, biocompatibility, and budget-friendly substance [9]. The existence of abundantly functioning groups, specifically amine and hydroxyl, in the polymer's scaffold facilitates active receptor sites to adsorb metal ions more proficiently. Chitosan possesses a unique structure that includes high-functioning groups, such as amino (-NH₂) and hydroxyl (-OH) groups, in its backbone. These functional groups serve as active sites for adsorption. The amino groups can act as Lewis bases, capable of forming coordination complexes with metal ions through ion exchange or chelation processes. The hydroxyl groups, on the other hand, contribute to the adsorption through electrostatic interactions, hydrogen bonding, and surface complexation [10]. Although chitosan-modified biochar has a higher adsorption capacity, it is necessary to perform time-consuming post-treatment activities such as sedimentation, centrifugation, and filtering to collect the solid particles that were filtered out of the treated water. Since it takes a long time for the low-density particles to completely settle, the recovery of these tiny particles from the huge industrial waste treatment tank becomes difficult. Therefore, the introduction of magnetic characteristics to the biochar-based adsorbent may further alleviate the challenging recovery of the biochar-based adsorbents from the water bodies. Magnetic impregnation of the biochar would increase the composite's reusability after modification. Many recent investigations have synthesized flexible composite adsorbents by combining magnetic particles and chitosan with biomass. As a bonus, the introduction of magnetic species may attract additional metal ions owing to its superior conductivity, making magnetic separation a win-win technique for recovering adsorbent from an aqueous medium. Magnetic biochar and chitosan, when combined, provide an excellent composite for cleaning up secondary pollution by removing a wide range of metals [11]. The current research on the utilization of chitosan for surface modification of biochars to improve their ability to apprehend heavy metals is still limited. This combination shows enormous potential as it effectively utilizes the perks of biochar and chitosan, resulting in significant benefits for binding Cr (VI). Fe₂O₃ particles are very useful in the treatment of wastewater due to their accessible cost and ease of separation. They have been used to effectively remove heavy metals and organic pollutants [12].

Biomass adsorbents are widely applied as secret weapons for the sustainable adsorption of environmental toxicants. The green sorbents prepared by biomass are invaluable tools for unlocking the power of waste by reducing the cost of remediation techniques for safe water. This research explores the efficacy of removing Cr(VI) using crosslinked chitosan hydrogel immobilized with magnetic biochars created from peanut shells by pyrolytic technique. Scanning electron microscopy (SEM), Fourier transform infrared (FTIR) analysis, X-ray photoelectron spectroscopy (XPS), and (Brunauer- Emmett-Teller) BET analysis were all collectively used to characterize the generated material. The adsorption property of chitosan-modified magnetic biochar for Cr(VI) in aqueous solution was also studied by examining the effects of pH, kinetics, and sorption isotherms.

2. Material and methods

2.1. Materials

Chitosan powder (85 % acetylation degree) was purchased from Alfa Aesar suppliers in, the USA. (Lot No A2041604). Peanut shells were collected from locally available fields to make pristine biochar. Ferric chloride hexahydrate, Glutaraldehyde (50 % V/V), acetic acid, Sodium hydroxide, potassium dichromate and 1,5 diphenyl carbazide (DPC) were purchased from Fisher Scientific, India. The solution was prepared using double-distilled water, and all of the chemicals utilized in the experiment were of the analytical reagent grade.

2.2. Incorporation procedure of Fe_2O_3 -biochar composite

The collection of peanut shells and synthesis of biochar pyrolytically was referred to in our previously published literature [13], herein, slight modifications were applied to obtain a magnetic biochar composite. According to the standard procedure, the dried peanut shells were crushed into micron-sized particles in a domestic mixer grinder before being sieved via a sieved shaker machine to produce a 70–80 mesh screen. The next step included soaking 25 grams of totally dried and powdered biomass in 80 mL of a 2M $FeCl_3$ solution. For 0.5 hours, the solution was continuously stirred using a magnetic stirrer at room temperature. After that, the mixture was aged for an additional 0.5 hours at 70 °C to speed up hydrolysis and Fe^{3+} precipitation. After that, the pre-treated biomass sample was placed in an alumina crucible and heated in a vacuum-applied muffle furnace at temperatures of 250, 350, 450, and 550 °C with rises

of 10 °C per minute and retention times of 10 minutes at each level while N_2 was continuously pumped in at a rate of 20 mL min^{-1} . The sample was kept at the same temperature after reaching 550 °C for two hours in an oxygen-free atmosphere. After finishing the process, the furnace's temperature naturally dropped to room temperature. The dried material was then ground and sieved to produce magnetic biochar that had a particle size of less than 0.5 mm. The dedicator held the prepared material. The finished product is known as a PSB/ γ - Fe_2O_3 composite (yield 38.5%).

2.3. Preparation of chitosan functionalized Fe_2O_3 -biochar composite

Chitosan powder (8.0 g) was first dissolved in 2% (v/v) acetic acid (500 mL) to obtain a homogenized viscous chitosan solution under continuous stirring for 2 h at 50 °C. Afterwards, 4 g of PSB/ γ - Fe_2O_3 composite was added to 50 ml of chitosan solution and the compounds were reacted in the ultrasonic bath for 30 min at 40 °C. 10 mL glutaraldehyde (25 % in H_2O) was then injected dropwise very slowly into the reaction system. After 30 min, keeping at 40 °C, NaOH solution (0.1 M) was added dropwise into the mixtures until the pH value reached 9. The solution was then allowed to stand as such in a Petri dish and undisturbed for the next 24 hours. A soft cross-linked three-dimensional network structure of chitosan-coated biochar magnetic hydrogel was formed and the solution turned light yellow to brownish yellow. The prepared chitosan hydrogel was then thoroughly washed with milli-Q water several times to remove any unreacted monomer. The final product was named CH@PSB- γ - Fe_2O_3 composite. The detailed preparation process is shown in Figure 1.

2.4. Characterization methods

Standard spectroscopic methods were leveraged to explore the structural peculiarities of the synthesized material. Fourier-transform infrared spectroscopy (FTIR) (Perkin Elmer) with a working range of 4000-400 cm^{-1} provides verified existence of abundant functional groups and some morphological alteration resulting from the incorporation of chitosan onto the surface of magnetic biochar. Exterior aesthetics and microstructure were analyzed by Scanning electron microscope (Carl Zeiss, Germany, model: Zeiss Gemini 300). The crystalline structure was examined by an X-ray diffractometer (Panalytical XPERT-PRO, UK) with 2θ range from 5° to 98° at a wavelength of 1.54059 Å. Energy dispersive X-ray spectrum (EDS) was obtained for elemental compositions as a crucial tool for unravelling materials' composition

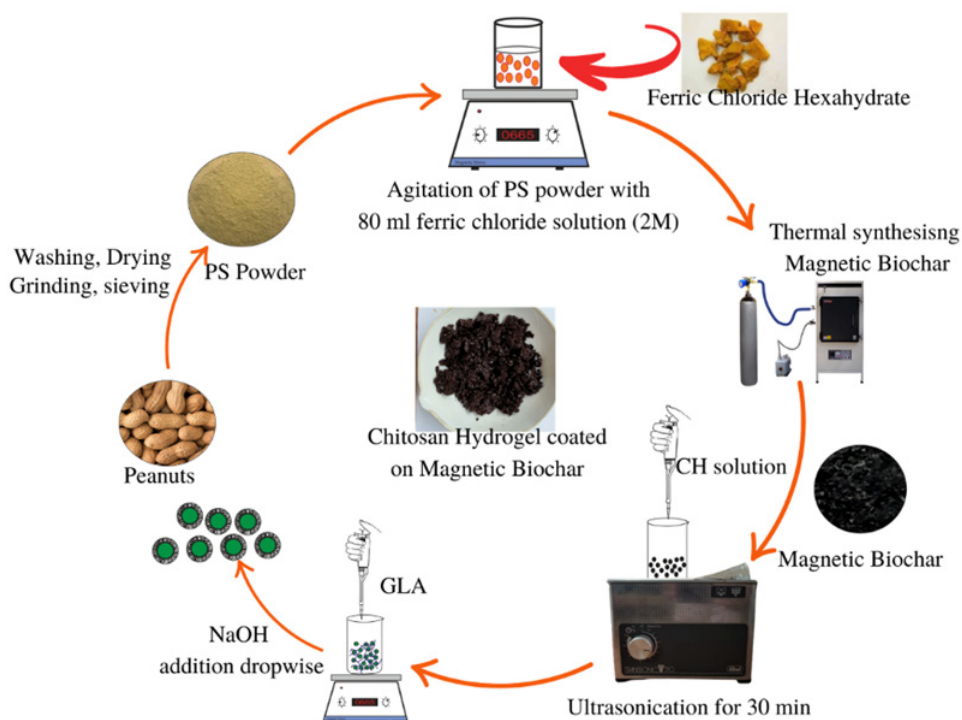


Fig. 1. Schematic presentation for synthesizing CH@PSB/ γ -Fe₂O₃

and structural characteristics, shedding light on their chemical makeup and potential interactions. XPS spectra (Scienta omicron, Germany,) furnished with Al K_α X-ray source (1486.7 eV) in ultra-high vacuum were used to determine the surface composition, relative abundance of these compositions and surface chemical structure of the prepared adsorbent. The point of zero charges (PZC) is the location where the total amount of positive and negative charges on the surface of a substance is equalized. The surface exterior gets negatively charged above the PZC and positively charged below it. The surface area and pore size distributions of PSB/ γ -Fe₂O₃ and CH@PSB/ γ -Fe₂O₃ were calculated using the Barrett-Joyner-Halenda (BJH) model and the Brunauer-Emmett-Teller (BET) equation, respectively (quantachrome V5.21 adsorption analyzer). The samples were degassed for 5.3 hours at 200 °C and weighed around 0.0442 mg. To get pore size distributions and BET surface area, BET and BJH interpretations were then applied using the N₂ adsorption-desorption isotherm at 77.35 K.

2.5. Chromium Adsorption study through batch system

Chromium (VI) reference solutions (100 mL) of varied quantities were imparted with a predetermined amount of adsorbent in Erlenmeyer flasks of 250 mL

for every single batch experiment. Adsorption activity was then assessed at a predetermined contact time at room temperature using an orbital agitator with a 140 rpm shaking speed. Once the solutions had reached equilibrium, they were all collected from the flask, traversed through a micron filter, and the quantity of remanent chromium content in the mixture was quantified using a spectrophotometer (Perkin Elmer, Lambda 850). In the experimental method, calibration standards were meticulously prepared by determining absorbance peak by scanning through wavelength range from 190 to 800 nm for known samples of chromium ranging from 0.2 to 8.0 mg L⁻¹. DPC (Diphenyl Carbazide) method was used to determine the absorbance peak calorimetrically by the reaction of 1,5 Diphenyl Carbazide with dissolved hexavalent chromium solution to produce red-violet complex in an acidic medium (pH= 2.0 ± 0.5) [14]. The Maximum absorbances were measured at 543 nm against the reagent blank, Hence, this wavelength was selected to determine the absorption peak for equilibrium chromium content during all the experiments. The procedure was carried out in standard 10 mm quartz cuvettes in triplicate. The average absorbance was calculated, and a calibration curve was plotted. Validation of the analytical method was performed by finding the linearity range, detection limit (LOD), quantification limit (LOQ), relative standard

deviation (%RSD) and recovery percentage to verify the absence of interference as per recommendations of IUPAC [15].

Batch systems were set in a way to evaluate the impact of contact durations (5, 10, 20, 30, 60, 90, and 120 min), pH (ranging from 2-12), the effect of coexisting ions, ionic strength and reusability of the prepared material. Sorption results for hexavalent chromium onto CH@PSB/ γ -Fe₂O₃ were expressed in terms of dismissal efficacy (%) and uptake capacity (mg g⁻¹) using Equations (1 and 2).

$$\text{Removal efficiency (\%)} = \frac{[C_i - C_t]}{C_i} \times 100 \quad (\text{Eq.1})$$

$$\text{Adsorption capacity } q_e \text{ (mg g}^{-1}\text{)} = \frac{[C_i - C_t]}{m} \times V \quad (\text{Eq.2})$$

In the given formula, m represents adsorbent mass (gram), C_i and C_t signify the initial and residual chromium concentrations (mg L⁻¹) observed at time t (min), and V stands for volume (L) in a batch study.

2.6. Adsorption isotherm

Adsorption isotherms reflect the correlation between the concentration of a substance in either a gas or liquid phase and the quantity becomes adsorbed onto a solid surface when equilibrium is reached. The Langmuir and Freundlich isotherm models were utilized for calculating removal capacity. These models aid in comprehending the equilibrium connection between the quantity of chromium adsorbed onto the adsorbent at a certain temperature and the initial concentration of chromium in the solution. Isotherm equilibriums were studied for the varied concentrations of 100 mL chromium solution tested for 150 minutes stirring at ambient temperature with an optimum pH level of 4 by introducing 0.5 g adsorbent. The equilibrium concentration of chromium was determined spectrophotometrically. The Langmuir isotherm is often used to describe monolayer adsorption on a homogenous surface. It was adopted for adsorption to occur at specific sites on the adsorbent surface, and each site can adsorb only one sorbate ion [16]. The Freundlich isotherm is an empirical model focused on adsorption likely to occur on heterogeneous surfaces with varying adsorption energies [17,18].

Linear form for Langmuir and Freundlich isotherm equations were employed to describe the equilibrium

adsorption parameters using Equations (3) and (4), respectively:

$$\text{Langmuir Equation: } \frac{1}{q_e} = \frac{1}{q_m} + \frac{1}{q_m K_L C_e} \quad (\text{Eq. 3})$$

$$\text{Freundlich Equation: } \log q_e = \log K_f + \frac{1}{n} \log C_e \quad (\text{Eq. 4})$$

Where q_e is the maximum adsorption capacity (mg g⁻¹) of the prepared adsorbent, C_e is the equilibrium concentration of chromium (VI) (mg L⁻¹). K_L and K_f are Langmuir and Freundlich constants, respectively.

2.7. Adsorption kinetic study

The field of kinetic investigation pertains to examining the temporal evolution of chemical reactions or processes. The study utilized various kinetic frameworks to analyze the mechanisms of mass transfer and chemical reactions associated with adsorption. Adsorption occurs when an adsorbate molecule interacts with an active site on the surface of an adsorbent molecule. The study employed to estimate pseudo-first and pseudo-second-order models. Through examining adsorption kinetics, valuable insights associated with the efficacy, ideal circumstances, and fundamental mechanisms of the aforementioned process were explored [19]. To comprehend the process of sorption on CH@PSB/ γ -Fe₂O₃, the experimental data was subjected to fitting using Lagergren's pseudo-first and pseudo-second order kinetics [20]. The Concentration of collected Chromium (VI) mixed with adsorbent material was determined spectrophotometrically at different time intervals of 2-120 min. The adsorption capacities provided at different times served as input for pseudo-first and pseudo-second order kinetics expressed as Equations (5) and (6), respectively:

$$\text{Log}(q_e - q_t) = \text{Log} q_e - \frac{K_1 t}{2.303} \quad (\text{Eq. 5})$$

$$\frac{t}{q_t} = \frac{1}{K_2 q_e^2} + \frac{t}{q_e} \quad (\text{Eq.6})$$

Where, and are adsorbed quantity (mg g⁻¹) of chromium (VI) at equilibrium and at time t, respectively. K₁(min⁻¹) and K₂(g mg⁻¹min⁻¹) are

adsorption rate constants for pseudo-first and pseudo-second kinetics. Traditional linear plots will be obtained for both the mechanism and to predict the reliability of the study, A linear regression algorithm was applied for optimization analysis.

2.8. Linear Regression analysis

The most frequent statistical technique for evaluating the model's validity is the linear regression coefficient. It statically measures the average functional relationship between variables. Also, it measures the degree of dependence of one variable on the other(s). It can be represented as blow Equations 7 and 8.

$$R^2 = 1 - \frac{SS_{Residual}}{SS_{Total}} \quad (\text{Eq.7})$$

$$SS_{residual} = \sum_{i=0}^n (q_{e,i} - q_{model,i})^2 \quad (\text{Fig. 8a})$$

$$SS_{total} = \sum_{i=0}^n (q_{e,i} - \bar{q}_{e,i})^2 \quad (\text{Fig. 8b})$$

$$\bar{q}_{e,i} = \frac{1}{n} \sum_{i=0}^n q_{e,i} \quad (\text{Fig. 8c})$$

Where, q_i and $q_{model,i}$ have experimentally obtained data and isotherm model prediction, respectively. For i th data point where n in the number of experimental data point.

2.9. Regeneration of adsorbent material

To evaluate the reusability of the synthesized adsorbent, six repeated cycles of sorption-desorption assays were tested. 100 mg of adsorbent was added to 100 ml Cr (VI) (100 mg L⁻¹) for agitating at 140 RPM at 27°C for 12 hrs. After each agitation, adsorbent particles were separated from the suspension by a micron filter and washed thoroughly with desorption reagent (0.1 HNO₃) followed by double deionized water and then dried at 80°C. The regenerated adsorbent was reused for the next cycle of the sorption process.

2.10. Influence of co-existing ions

The adsorption effectiveness may be considerably impacted by the presence of other ions in the solution. Since the ultimate goal is the treatment of industrial effluents, which will most probably contain other ions (like Cl⁻, NO₃⁻, SO₄²⁻, Na⁺, Mg²⁺ etc.) along with heavy metal ions, an efficient adsorbent is expected to retain its high adsorption capacity even in the presence of other ions. For determining the effect of the presence of other ions, the adsorption efficiency with the prepared adsorbent was checked at two different concentrations (1 ppm and 10 ppm) of NaCl, and NaNO₃, Na₂SO₄, Na₂(PO₄)₃ along with chromium ions.

3. Result and Discussion

3.1. Characterization of Prepared Composite

X-ray diffraction (XRD) can provide a comprehensive understanding of the phase structural features of CH@PSB/γ-Fe₂O₃. As illustrated in Figure 2 (a) the XRD patterns of pristine chitosan (CH) (85 % DDA) showed one strong and a weak reflection at 2θ=10.08° and 2θ= 20.22° respectively which reflects about amorphous crystal structure. The XRD spectrum patterns of PSB/γ-Fe₂O₃ exhibit several pairs of diffraction peaks in a range of 2θ° ~ 65° as Figure 2(b). Based on the JCPDS Card No. 19-0629, the distinct peaks at certain angles located at 24.38°, 33.38°, 35.38°, 41.14°, 49.14°, 54.26° and 62.60° corresponding to the (012), (104), (110), (113), (024), (116), and (214) crystal planes respectively, are the characteristics for Fe₂O₃ deposition on the PSB surface [21]. However, no apparent differences were observed for PSB/γ-Fe₂O₃ and CH@PSB/γ-Fe₂O₃ (Fig. 2c). The resulting XRD patterns were analyzed with peak shifting and lower peak intensity suggesting reduced crystallinity in CH@PSB/γ-Fe₂O₃ due to interaction of chitosan polymer. The weaker diffraction signals compared to the well-ordered crystalline for PSB/γ-Fe₂O₃ composite are due to the coating of chitosan on the Fe₂O₃-biochar surface. Chitosan typically contains amorphous regions, which might contribute to low intense diffraction peaks in the diffractograms. These amorphous regions could mask or dampen the intensity of the crystalline peaks from the magnetic biochar. Additionally, the peak shifts indicate alterations in the lattice parameters or crystallographic arrangement caused by the introduction of chitosan. These results suggest that chitosan was successfully immobilized with PSB/γ-Fe₂O₃ surface. FT-IR spectra for the pristine chitosan, PSB/γ-Fe₂O₃, and CH@PSB/γ-Fe₂O₃ are shown in

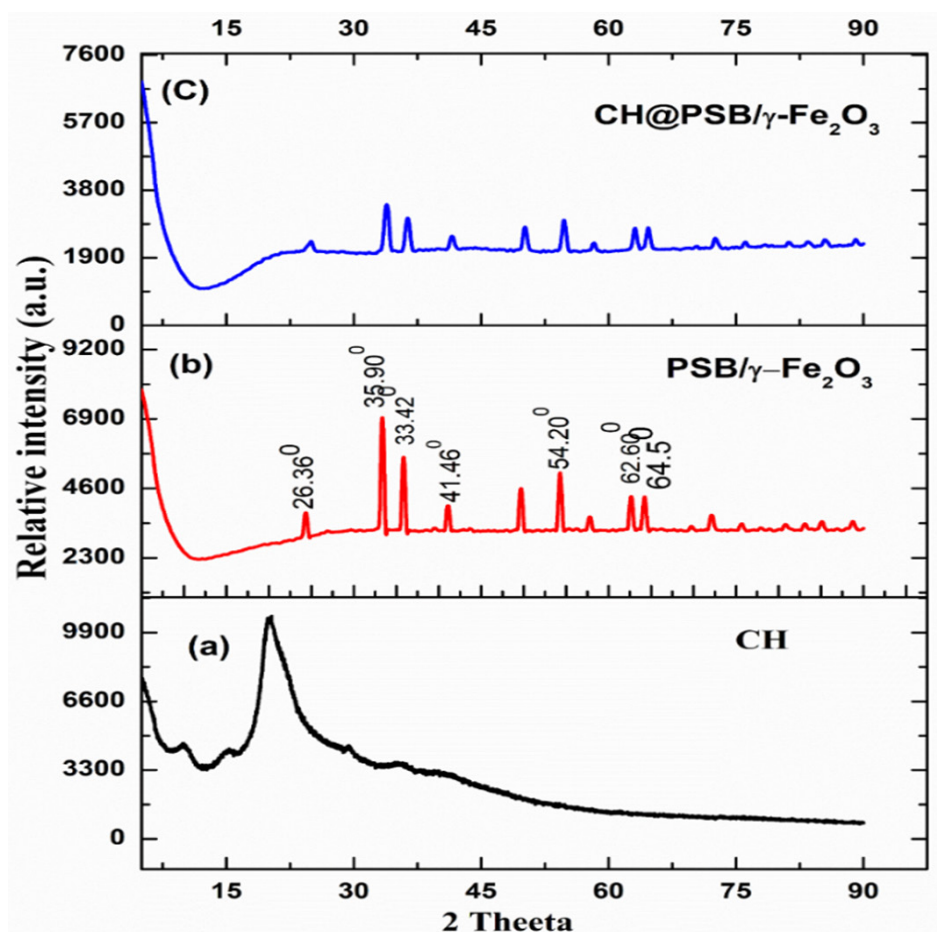


Fig. 2. XRD patterns for CH (a); PSB/ γ -Fe₂O₃ (b); and CH@PSB/ γ -Fe₂O₃ (c)

Figure 3. The absorption band at 3200~3600 cm⁻¹ is attributed to the -OH and N-H groups stretching vibration present in chitosan (Fig. 3a) but the intensity of these bands reduced after coating due to interaction of these functional groups with biochar surface (Fig. 3c). The band at 2931 and 2850 cm⁻¹ (Fig. 3c) was assigned for stretching vibration of aliphatic CH bond present in magnetic biochar [22]. The appearance of characteristic peaks around 1650-1550 cm⁻¹, attributed to the amide I and II bands corresponding to N-H bending and C-N stretching vibrations and the presence of a band at around 1027 cm⁻¹ related to the C-O stretching vibration are strong evidence of successful chitosan coating on the magnetic biochar surface. These peaks are specific to chitosan's polysaccharide structure and are not typically observed in the FTIR spectra of magnetic biochar. The peak at 1365 cm⁻¹ is often attributed to the bending vibration of the methyl (CH₃) groups. It indicates the presence of methyl groups in the composite, which could be associated

with either the chitosan component or the magnetic biochar. The peak at 1407 cm⁻¹ might be due to the presence of stretching vibration of the C-O bond in the -COOH group. In addition, a peak at 1653 cm⁻¹ is related to the amide I band, which arises from the C=O stretching vibration of the amide (CONH) bonds in chitosan. It confirms the presence of chitosan in the coated biochar sample. The peak at 1605 cm⁻¹ in Fe₂O₃-biochar composite (Fig. 3b) was attributed to vibrations involving metal-oxygen bonds which disappeared after reacting with chitosan suggesting a significant change in the composition or structure of the material due to the chemical interaction with composite and surface coverage. The detection of the aforementioned peaks confirms the successful incorporation of chitosan onto the biochar surface, validating the formation of the chitosan-magnetic biochar composite. Additionally, the disappearance of peaks at 1064 and 1150 cm⁻¹ in chitosan spectra (Fig. 3a) reveals that coating onto the magnetic biochar surface suggests significant

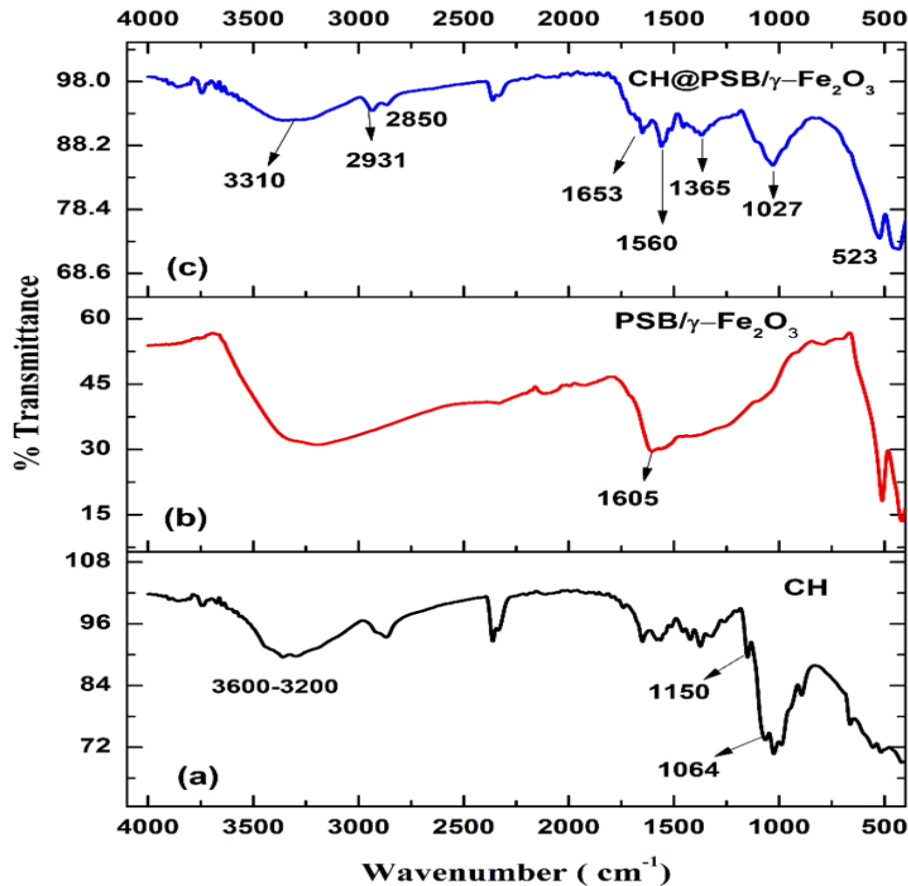


Fig. 3. FTIR spectra for Chitosan (a); PSB/ γ -Fe₂O₃ (b); and CH@PSB/ γ -Fe₂O₃ (c)

changes in the chitosan's chemical environment which involves chemical interactions, cross-linking, hydrogen bonding, conformational changes in the chitosan molecules. Furthermore, compared with chitosan polymer, in the spectrum of CH@PSB/ γ -Fe₂O₃ a new strong peak located at 527 cm⁻¹ was attributed to the Fe-O lattice vibrations of Fe₃O₄. This indicates the presence of Fe₃O₄ particles in the prepared sample [23]. Notably, the functional groups of CH@PSB/ γ -Fe₂O₃ were different from those of pristine chitosan and magnetic biochar, which impacted its subsequent adsorption ability. Magnetic biochar made from ferric chloride has distinctive characteristics in its surface morphology. As shown in Figure 4 (b), it generally has a porous structure with a variety of pore sizes and internal mesopore distributions, which increases its surface area and adsorption capacity. The breakdown of lignocellulosic material at high temperatures was linked to the production of a sequence of cracks on the surface of biochar, which caused volatile

chemicals to evaporate from the newly created pores. Some shimmering developed on the surface of PSB/ γ -Fe₂O₃, indicating the existence of thick surface layering particles, which are composed of magnetic nanoparticles inserted during manufacturing. These magnificent particles might be incorporated into the porous surface of the biochar or scattered throughout it. Due to the carbonization process and the development of cracks and fissures, the surface seems uneven and rough. Figure 4 (d, e, and f) shows that chitosan coating on magnetic biochar may result in a reduction in pore volume or quantity when compared to uncoated magnetic biochar. This is mainly because the magnetic biochar's surface develops a layer of chitosan coating, which partly fills in the pores already present and decreases the volume of those pores. However, CH@PSB/ γ -Fe₂O₃ had a higher sorption capacity than PSB/ γ -Fe₂O₃, indicating that the adsorption process was predominantly dependent on the functional groups rather than the surface pore structure.

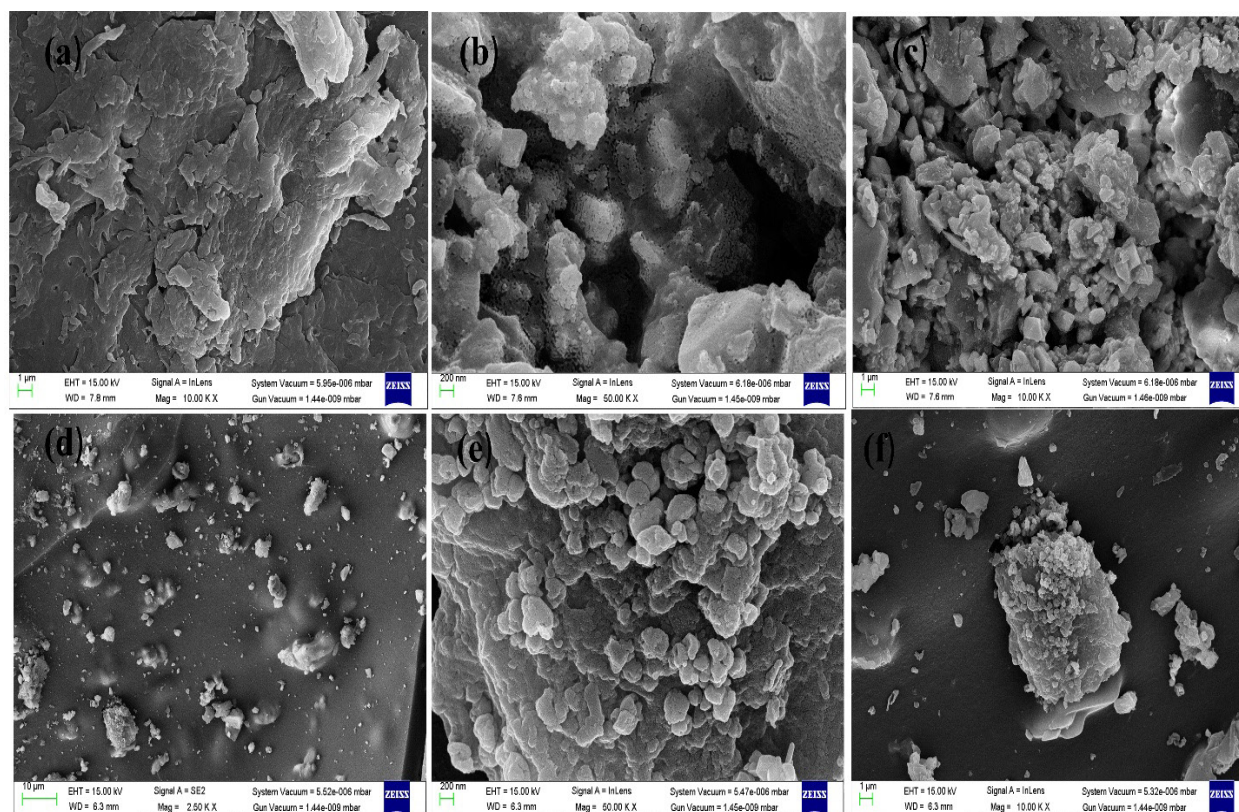


Fig. 4. SEM images of Pristine chitosan (a); PSB/ γ -Fe₂O₃ (b, c); and CH@PSB/ γ -Fe₂O₃ (d, e, f)

EDS results for Chitosan (CH), magnetic Biochar (PSB/ γ -Fe₂O₃) and chitosan-coated magnetic biochar (CH@PSB/ γ -Fe₂O₃) offer a glimpse into their composition and potential structural modifications. In this study, we delve into the variations in C, N, O and Fe contents across Fe₂O₃/biochar, chitosan-coated Fe₂O₃ biochar, and pure chitosan. From Figure 5 (a, b, and c) EDS of the prepared material showed remarkable transformation after coating of chitosan onto magnetic biochar. The CH@PSB/ γ -Fe₂O₃ displays a significant increase in carbon content, reaching 57.7% as compared to PSB/ γ -Fe₂O₃ (25.8%) This enhancement is indicative of the successful incorporation of chitosan onto the biochar surface. Observed carbon content in pure chitosan of 42.3%. The distinctive increase in carbon content observed in the CH@PSB/ γ -Fe₂O₃ sample corroborates the successful interaction between chitosan and the biochar matrix. The decline in nitrogen content in the CH@PSB/ γ -Fe₂O₃ sample (0.9 %) compared with PSB/ γ -Fe₂O₃ (3.3 %) suggests that the chitosan coating process has led to modifications in the nitrogen composition of the composite material. The results for BET surface analysis are shown in Table

1 the results were compared with BET analysis of pristine biochar made from peanut shells with Fe₂O₃ and crosslinked chitosan-loaded samples showed a significant reduction in surface area as well as pore volume and pore size. The reduction is due to the aggregation of Fe₂O₃ nanoparticles and chitosan on to surface. While the reduction in surface area, pore size, and volume might seem unfavourable, the addition of chitosan onto the magnetic biochar surface might enhance specific functionalities of the material's behavior for targeted adsorption.

With the intent of deeper insight into the surface chemical and elemental composition of the prepared adsorbent, XPS survey spectra were recorded and analyzed according to Figure 6 (a to d). As illustrated in Figure 6a, XPS survey spectra of CH@PSB/ γ -Fe₂O₃ find four significant peaks which revealed the presence of C 1s (283.5 eV), N 1s (396.5 eV), O 1s (531 eV) and Fe 2p (711.5 eV). It was further analyzed that the elemental composition of CH@PSB/ γ -Fe₂O₃ contains C (61.89 %), O (21.78 %), N (2.83 %) and Fe (8.08 %). The high-resolution spectrum for C 1s is deconvoluted in Figure 6b, revealing the existence

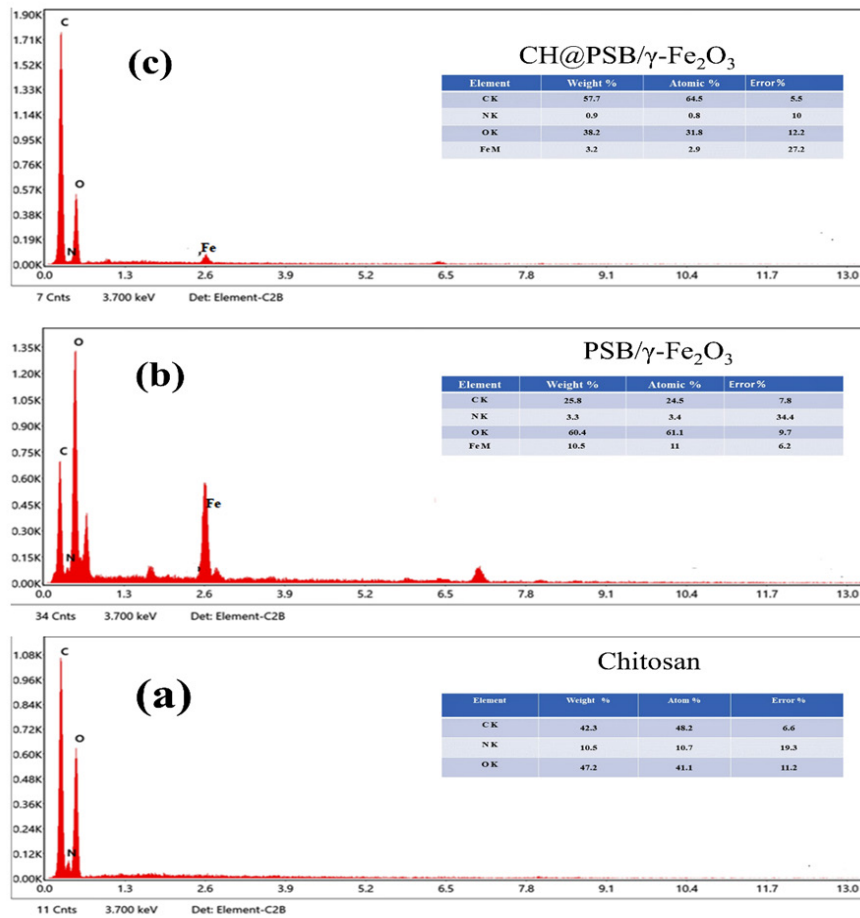


Fig. 5. EDS analysis of Chitosan (a); PSB/γ-Fe₂O₃ (b); and CH@PSB/γ-Fe₂O₃ (c)

Table 1. BET and BJH analysis results for prepared samples

Sample	S _{BET} (m ² g ⁻¹)	V _{micro} (cm ³ g ⁻¹)	Pore diameter (nm)
PS Biochar [13]	479.569	0.124	1.426
PSB/γ- Fe ₂ O ₃	340.252	0.958	1.053
CH@PSB/γ- Fe ₂ O ₃	98.788	0.875	0.756

PSB: Peanut shell biochar

of carbon in three different functional groups: C-N (283.84 eV), C-C (284.64 eV), C-O (286.72 eV). The high-resolution spectrum of O 1s [Figure 6c] finds two deconvoluted peaks with binding energies at 531.59 (eV) and 529.24 (eV) corresponding to C=O and C-O functional groups, respectively. The high-resolution XPS spectra of Fe 2p of CH@PSB/γ-Fe₂O₃ exhibited four peaks: 723.77 eV could be assigned for Fe 2P_{1/2}; 709.71 for Fe 2P_{3/2}; and peaks corresponding to binding energies at 718.02 and 713.71 may be associated with

shake-up or satellite peaks which are characteristics of Fe in Fe₂O₃. The XPS results of chitosan-coated magnetic biochar indicated the potential appearance of the iron oxides, reduced iron species, interacting with chitosan polymer. Figure 7a illustrates the zero point charge of CH@PSB/γ- Fe₂O₃ is located at 4.5 pH. As a result of the protonation of the amine group in chitosan, the adsorbent's surface acquires a positive charge below this pH, which is favorable for the adsorption of negatively charged entities.

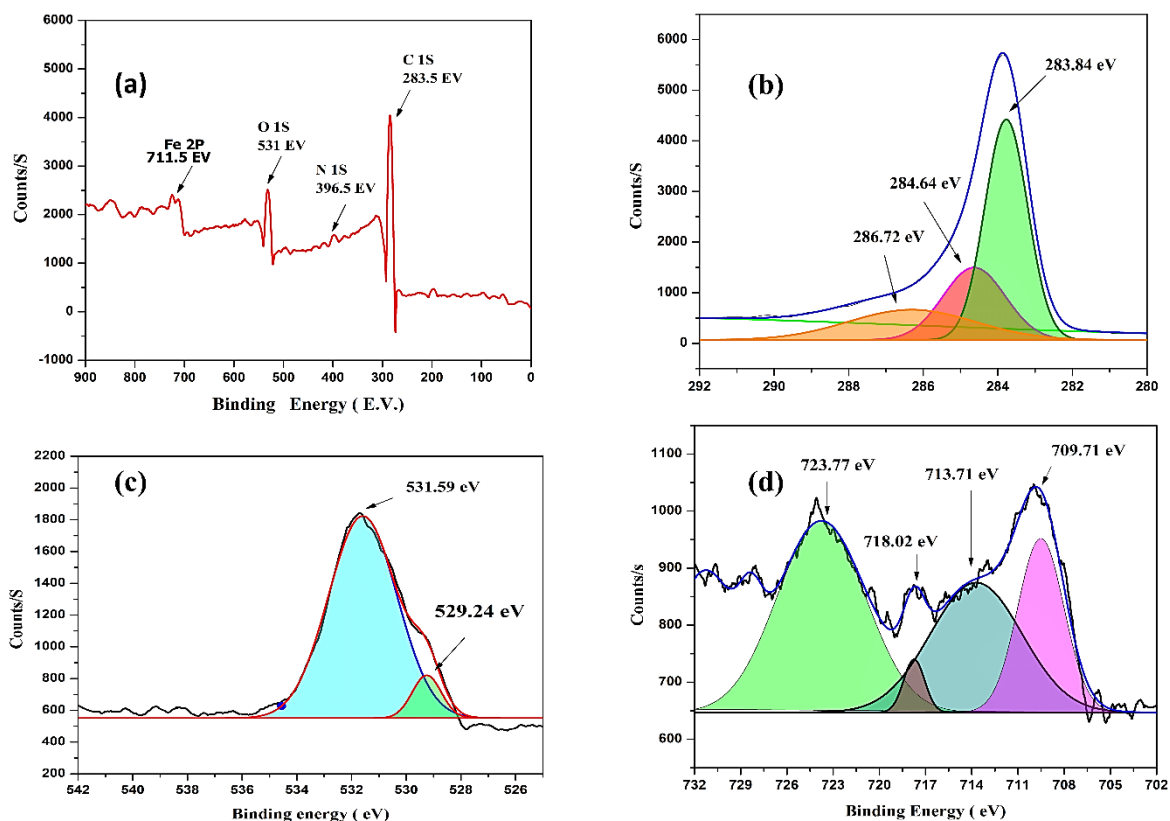


Fig. 6. XPS Survey Spectra of CH@PSB/ γ -Fe₂O₃ (a); High resolution XPS spectra of C 1s (b); O 1s (c); Fe 2p (d)

3.2. Adsorption studies for chromium

3.2.1. Consequences of changing solution pH

The adsorption of chromium by CH@PSB/ γ -Fe₂O₃ can be significantly influenced by the pH of the solution. When pH is less than 6.8, HCrO₄⁻ becomes major speciation but at pH more than 7.2, Cr (VI) ions can form negatively charged oxyanions such as chromate (CrO₄²⁻) and dichromate (Cr₂O₇²⁻). The point of zero charge for CH@PSB/ γ -Fe₂O₃ was located at 4.5 pH (Fig. 7a). Adsorption studies are typically conducted at varied ranges of pH to determine the optimal conditions for efficient chromium removal. Sorption capacity for Cr (VI) notably declined from 85.2 mg g⁻¹ to 24.6 mg g⁻¹ with the change in pH value from 2 to 8 as depicted in Figure 7b. Sorption performance for the produced composites was found to be boosted at lower pH value, mainly due to enhanced electrostatic attraction created by protonated amino functional groups on chitosan. At higher pH, the negatively charged surface of adsorbent material impeded chromium sorption due to electrostatic repulsion among (CrO₄²⁻) and OH⁻. Figure 8 illustrates the process of chromium adsorption by sorbent material.

3.2.2. Influence of Ionic Strength on Adsorption

The sorption behaviour of chromium by CH@PSB/ γ -Fe₂O₃ was investigated in the presence of a varied concentration of NaNO₃ and results were exhibited as decreasing adsorption capacity from 83.6 to 30.1 mg L⁻¹ (Fig. 9). With increasing NaNO₃ strength from 0.05 M to 2M maintaining pH at 4.0, suggesting supersession in Cr (VI) sorption at elevated ionic strength. This was primarily due to the competitive sorption of nitrate ions onto CH@PSB/ γ -Fe₂O₃.

3.3. Adsorption Equilibrium Analysis

The adsorption capacity for the prepared material was evaluated using the two most universally adopted Langmuir and Freundlich isotherm models. The pertinent reports are provided in Table 2 and Figure 10 (a and b) are illustrated for validity of the models. The linear fitting of the observed data based on origin pro 8.5 software revealed that the performance of CH@PSB/ γ -Fe₂O₃ was better fitted by the Langmuir equation with a correlation factor (R²) of 0.9998. These findings demonstrated the monolayer adsorption process and Equation 3 was used to determine the maximum adsorption capacity (Q_{max}) as 14.285 mg g⁻¹.

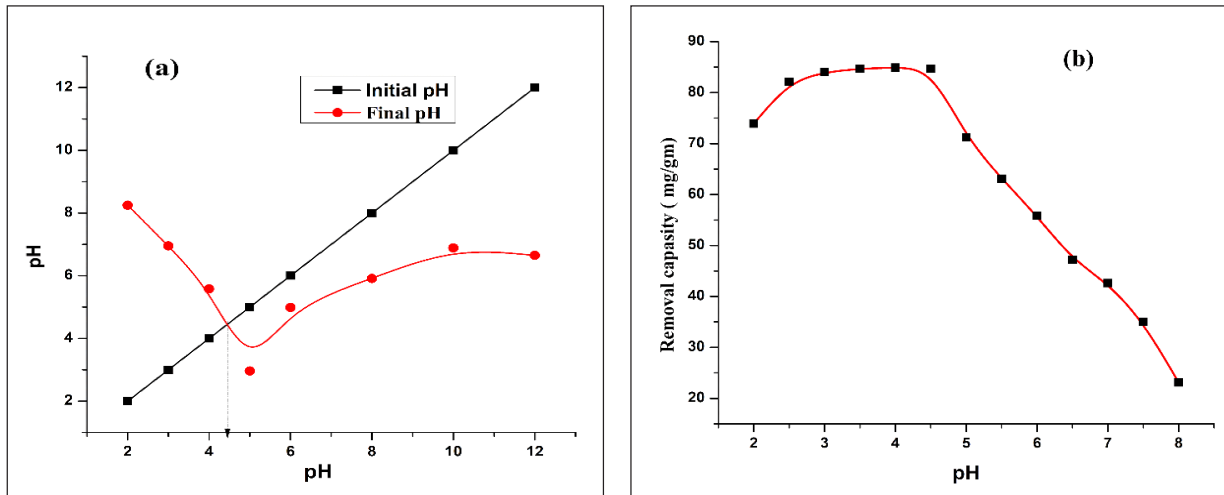


Fig. 7. Zero-point charge (a); and effect of zero-point-sorption of chromium onto CH@PSB/ γ -Fe₂O₃ (b)

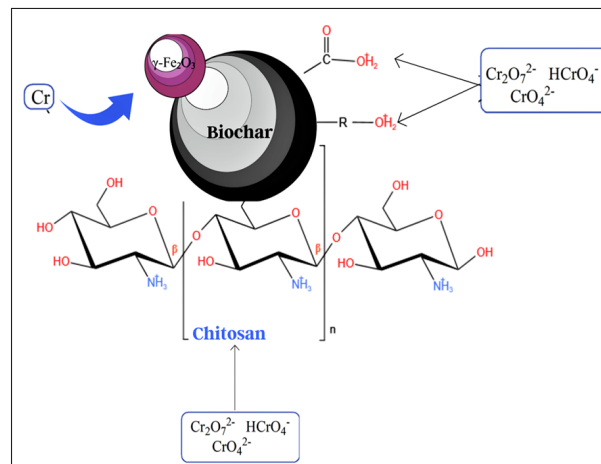


Fig. 8. Strategic Representation of Chromium Adsorption onto CH@PSB/ γ -Fe₂O₃

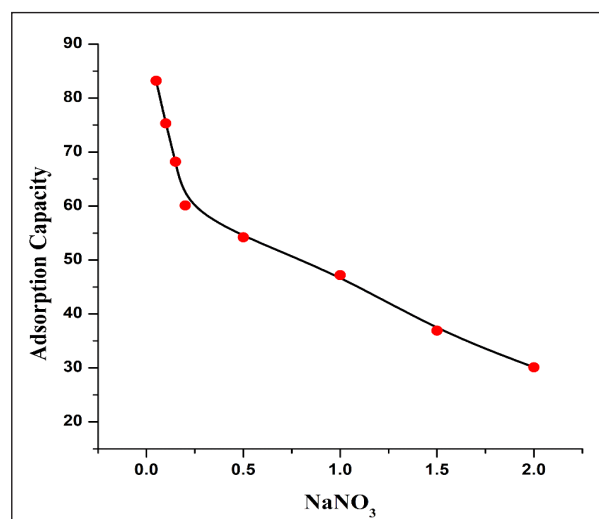


Fig. 9. Effect of Ionic Strength

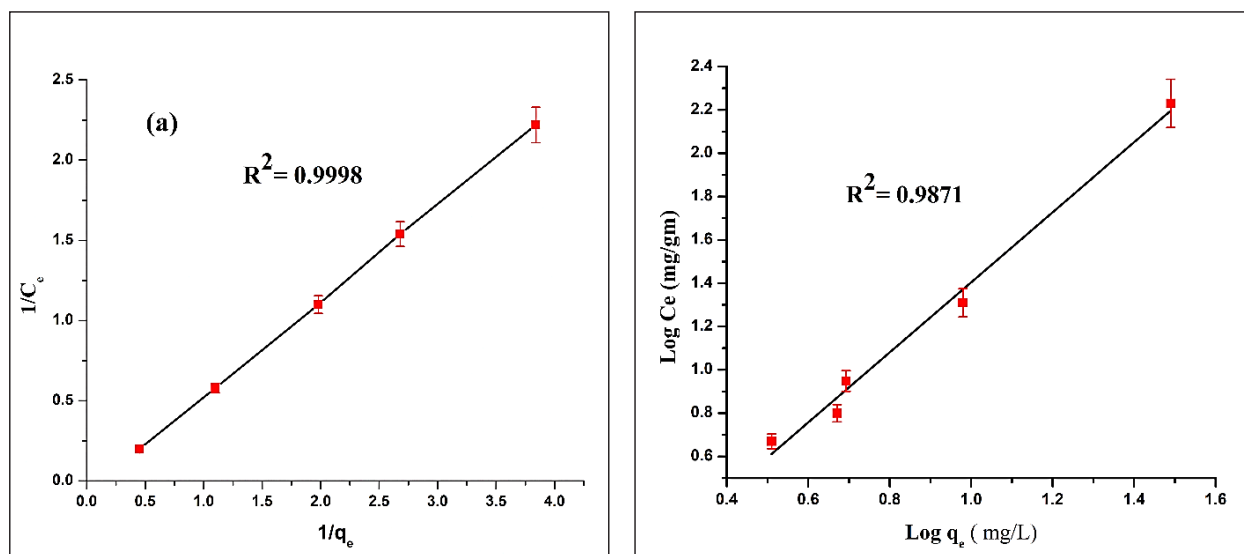


Fig. 10. Isothermal equilibrium study for chromium adsorption onto CH@PSB/ γ -Fe₂O₃ Langmuir (a); and Freundlich model (b)

3.4. Adsorption kinetics

Sorption rate is another consideration for studying adsorption capacity associated with contact duration. The sorption kinetic was investigated for 0 to 90 min of contact time. As shown in Figure 11 sorption occurred rapidly for an initial 20 min of contact and then this trend slowly grew until it reached a plateau. Sorption equilibrium attained in just 40 min. The elevated abundance of adsorption surfaces may be assigned for the speedy progress in the initial adsorption rate of Cr (VI) [24]. Adsorption rates accordingly decreased as the number of accessible adsorption sites decreased over time. As a result, 40

minutes was shown to be an ideal contact time for the adsorption process. The sorption kinetics for pseudo-first and pseudo-second-order models were applied for chromium adsorption onto CH@PSB/ γ -Fe₂O₃ and corresponding results were evaluated in Figure 12 (a and b) and Table 2. The experimental findings of calculated parameters revealed that the data were best signified by the pseudo-second-order model (Table 2), with a correlation coefficient (R^2) of 0.9994 with an equilibrium sorption capacity of 83.33 mg g⁻¹. Kinetics consideration is suggested for surface adsorption and chemisorption mechanism in the rate-controlling step.

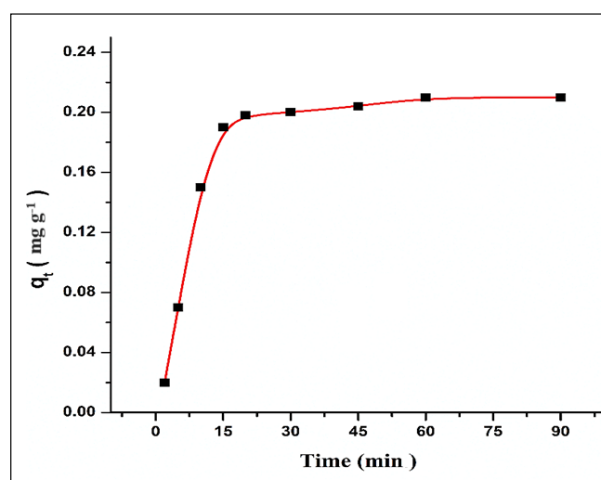


Fig. 11. Effect of time on adsorption of chromium onto CH@PSB/ γ -Fe₂O₃

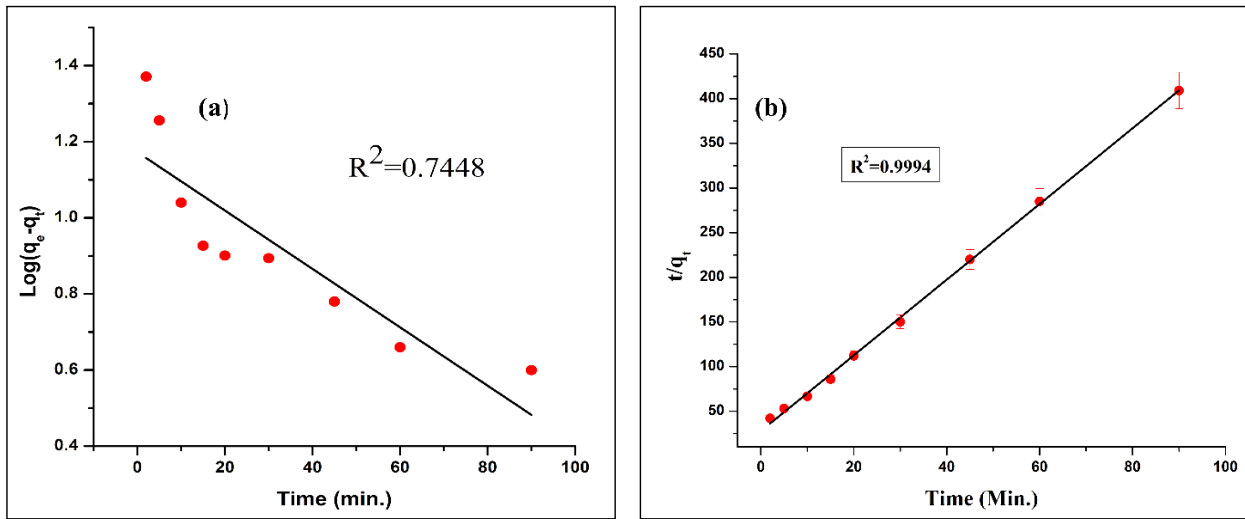


Fig. 12. Adsorption Kinetics for Chromium sorption onto CH@PSB/γ-Fe₂O₃: Pseudo-first (a); and Pseudo-second-order model (b) and Pseudo-second-order model (b)

Table 2. Adsorption isotherm and kinetic parameters for chromium adsorption onto CH@PSB/γ-Fe₂O₃

Langmuir constants			Freundlich constants			
K _L	Q _{max} (mg g ⁻¹)	R ²	K _F	n	R ²	
0.1170	14.285	0.9998	0.616	2.56	0.9871	
Experimental value	Pseudo first order			Pseudo second order		
Q _{e,exp.} (mg g ⁻¹)	K ₁ (min ⁻¹)	Q _{e, cal} (mg g ⁻¹)	R ²	K ₂ (g mg ⁻¹ min ⁻¹)	Q _{e, cal} (mg g ⁻¹)	R ²
0.168	0.0161	14.79	0.744	0.089	83.33	0.9994

Initial Chromium content:
2 mg L⁻¹; pH:4.0;
Temperature:28 0C;
Time:0-90 min@140RPM;
Adsorbent dose: 0.5g;
Solution volume: 100 mL

3.5. Reutilization of the adsorbent

Six consecutive iterations of sorption-desorption were tested for synthesized adsorbent to execute reusability. As demonstrated in Figure 13, removal efficiency gradually declined with every next cycle, and it dropped from 85 % to 26 % in the

sixth round. The material has excellent reusability for up to four cycles. Overall, the results of these recycled trials provide compelling evidence that the prepared CH@PSB/γ-Fe₂O₃ demonstrated excellent reusability and holds significant promise for practical applications.

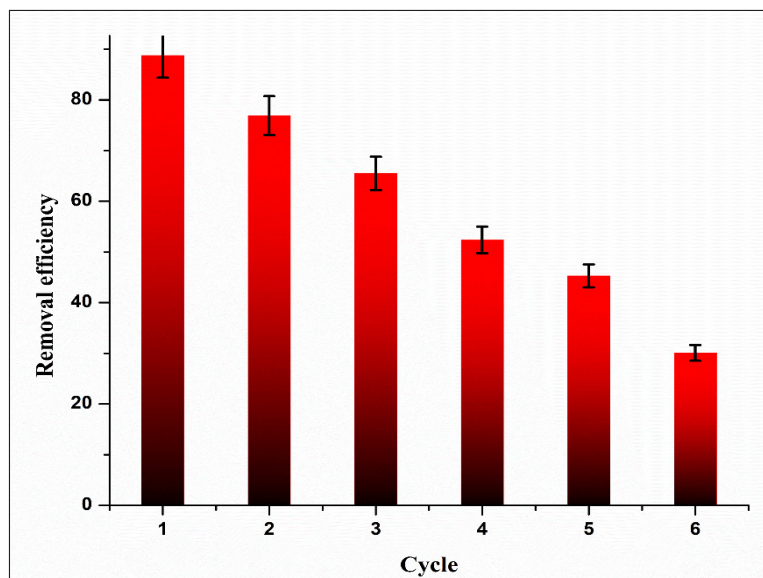


Fig. 13. Six sorption-desorption cycles for Cr (VI) adsorption onto CH@PSB/ γ -Fe₂O₃

3.6. Influence of coexisting ions on removal efficiency for real water samples

Drinking water can contain multiple ions as water sources often come into contact with geological formations, industrial activities, or other environmental factors. The synchronous presence of other ions can significantly influence the removal of chromium during water treatment. The interactions between these coexisting ions and chromium can affect the adsorption capacity, speciation, and overall efficiency of the removal process. Experiments were therefore carried out to learn how coexisting ions affect chromium removal in the presence of four ions

such as Cl⁻, SO₄²⁻, NO₃⁻, and PO₄²⁻ (for 1 ppm or 1 mgL⁻¹ and 10 ppm concentrations). The experimental observations (Fig.14) suggesting for consistent efficiency at approximately 80 % chromium removal by CH@PSB/ γ -Fe₂O₃ at 1 ppm solution. Except for PO₄²⁻ removal efficiency by coexisting ions was only minimally hampered. It is because of competitive interactions of anionic species with functional groups on modified chitosan. However, there is a weaker interaction for Cl⁻, SO₄²⁻, NO₃⁻ but due to the higher affinity of PO₄²⁻ ion with iron oxide its effect is high. In addition, as the concentration of coexisting ions increased to 10 ppm, this influence was higher.

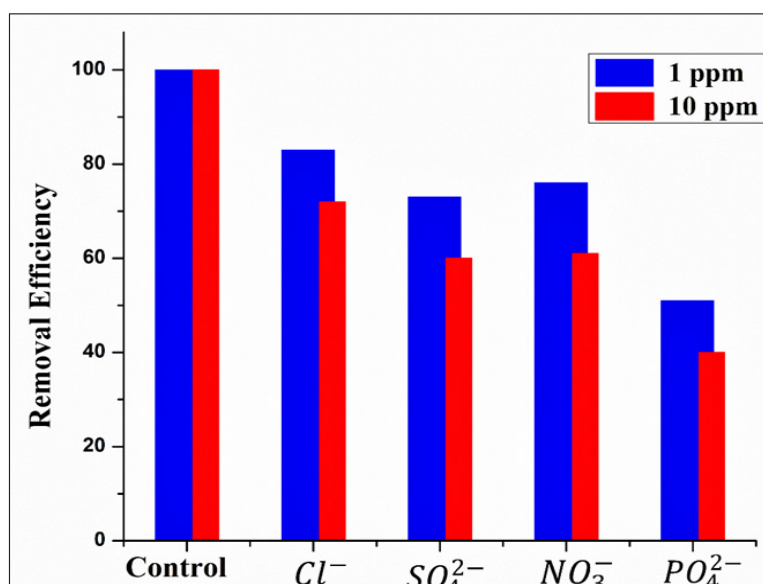


Fig. 14. Effect of coexisting ions in removing Cr(VI) using CH@PSB/ γ -Fe₂O₃

3.7. Validation of analytical method

The analytical data acquired for the spectrophotometric validity of the method are presented in Table 3. Using 100 mL solutions with increasing analyte concentrations (0.2 - 8 $\mu\text{g L}^{-1}$), the absorbance peaks and calibration curves were produced, as shown in Figures 15 (a) and 15 (b), respectively. All points of the calibration curve were subjected to the preconcentration procedure for the determination of Cr (VI) via the carbazide method as mentioned in the experimental part of this work. The calibration curve exhibits linearity in the range from 0.5 to 6 $\mu\text{g L}^{-1}$ with a regression coefficient (R^2) equal to 0.9976. Using seven consecutive measurements, the analytical approach presented in this research demonstrated high accuracy with a relative standard deviation (RDS) of 7.62%. The limit of detection (LOD), defined as the smallest amount of analyte that a method can detect, was

calculated to be 3 times the standard deviation obtained by 7 readings divided by the slope of the calibration curve. The quantification limit (LOQ), which expresses the actual amount of analyte in a sample with considerable precision and accuracy, was determined to be 10 times the standard deviation obtained by 7 readings divided by the slope of the calibration curve. The LOD was 0.65 $\mu\text{g L}^{-1}$ and the LOQ was 2.16 $\mu\text{g L}^{-1}$. The accuracy of the method was tested from three known concentrations of standard solution, and the results revealed good percent recovery (% R) of $92.8 \pm 0.5\%$ to $103.09 \pm 0.5\%$. A comparison of proposed methods and some of the published microextraction methods for extraction and determination of Cr ions are summarized in Table 4. The accuracy and LOD values of the present method, for the determination of chromium ions, are comparable to those reported in the literature [25–32].

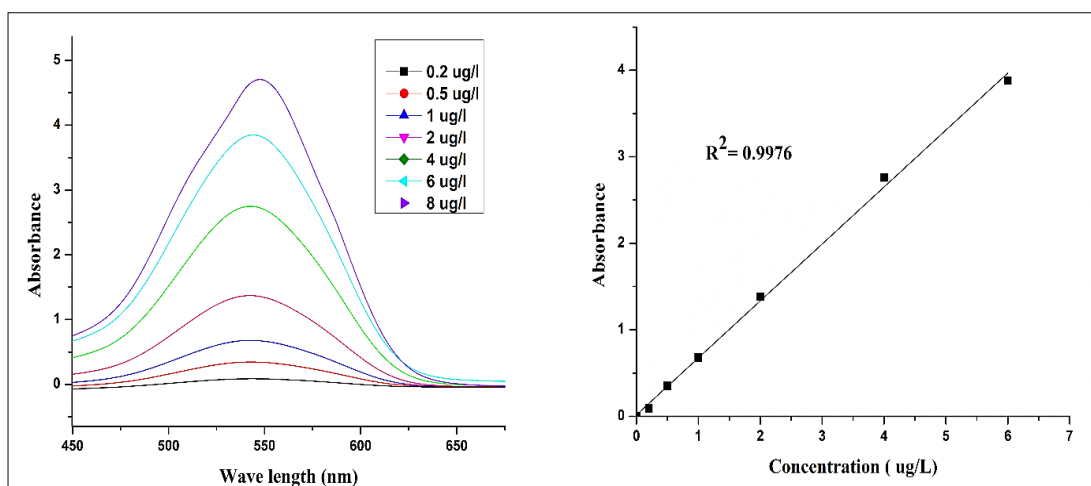


Fig. 15. UV Spectra for calibration standards (a); and calibration curve (b)

Table 3. Analytical validation parameters for Cr (VI) determination by proposed UV-VIS spectrophotometer

Characteristics	Validation Parameters
Calibration Curve	Values
Concentration Range ($\mu\text{g L}^{-1}$)	0.2-8.0
Absorbance Range	0.09-4.75
Wavelength Range (nm)	190-800
Slope	0.6583
Intercept	0.172
Regression Coefficient	0.9976
Regression Equation	$Y = 0.6583X + 0.172$
Validation Appearances	Values
Measurement wavelength (nm)	543
Linear Range ($\mu\text{g L}^{-1}$)	6.0 – 0.5
Limit of Detection (LOD) $\mu\text{g L}^{-1}$	0.65
Limit of Quantification (LOQ) $\mu\text{g L}^{-1}$	2.16
% Relative Standard Deviation (RSD)	7.62
% Recovery Percentage (R)	to 103.1 ± 0.5 0.5 ± 92.8

Table 4. Comparison of UV-Vis spectrophotometry using CH@PSB- γ -Fe₂O₃ to determine Cr (VI) in water with other studies of the literature

Detection method	LOD ($\mu\text{g L}^{-1}$)	Separation Technique	RSD (%)	Linear range ($\mu\text{g L}^{-1}$)	Recovery (%)	.Ref
SPE-FAAS		SPE	5 >	0.4-15	97 <	[25]
ETAAS	0.005	TSIL-DLLME	3.8	0.32 -0.02	105 -95	[26]
ETAAS	0.005	IICDET/LLME	3.8	0.02-1.75	98	[27]
ETAAS*	8.0	IL-DLLBME	4.3	0.03-4.4	104 -97	[28]
FAAS	7.1	SPE	2.7	20-700	88-110	[31]
Spectrophotometric	0.023	---	---	0.03-6.0	---	[32]
UV-Vis	0.65	DPC	7.62	6- 0.5	92-103	This work

FAAS: Flame Atomic Absorption spectrometry

SPE: Solid Phase Extraction

ET-AAS: Electro-Thermal Atomic Absorption Spectrometer

UV-Vis Spectrometry

*LOD=0.8 ng L⁻¹

4. Conclusion

In this study, a new adsorbent material was fabricated by immobilizing chitosan-coated iron oxide biochar for the effective desalinization of chromium ions from aqueous solution. Various spectroscopic studies confirmed the synthesis of a composite material comprising Fe₂O₃-biochar coated further with crosslinked chitosan. This hybrid material combines the magnetic properties of Fe₂O₃ with the porous structure of biochar, enhanced by the presence of chitosan. The successive coating of chitosan onto the Fe₂O₃-biochar surface adds a layer of complexity to the material's composition and properties, potentially impacting its surface area, porosity, and adsorption capabilities. This synthesized material holds promise for applications in the adsorption of chromium ions and the spectroscopic method used in the determination of chromium showed a LOD of 0.65 $\mu\text{g L}^{-1}$ with a recovery percentage of more than 92 %. The optimized pH for the highest removal capacity ($0.4 \pm 84.9 \text{ mg g}^{-1}$) is in the range of 3-5 pH. Additionally, there is a slight decrease in capacity with an increase in ionic strength. Langmuir isotherm equation fits well with adsorption data and the obtained removal capacity for CH@PSB/ γ -Fe₂O₃ exhibits 14.285 mg g^{-1} in batch system. The kinetic study suggests that pseudo-second-order is the best description of chromium adsorption onto CH@PSB/ γ -Fe₂O₃ suggesting a chemisorption pathway. The a slight decrease in removal efficiency in the presence of some other anions except for PO₄²⁻ ion. A reusability assay indicates for excellent utility of the prepared material for toxicant removal and more

than 50 % sorption capacity is retained for up to four cycles. In conclusion, the synthesized biosorbent is a novel green material for effective holds significant potential for wide-ranging applications in the field of Cr (VI) removal.

5. Acknowledge

Sardar Singh Poonia want to express his sincere gratitude towards CSIR (award no:09/098(0142)/2019-EMR-I) for providing support and financial aids in research. He would like to give special thanks to Head, Department of Chemistry for their exceptional support in providing the necessary resources.

6. Reference

- [1] L. Liu, W. Li, W. Song, M. Guo, Remediation techniques for heavy metal-contaminated soils: Principles and applicability, *Sci. Total Environ.*, 633 (2018) 206-219. <https://doi.org/10.1016/j.scitotenv.2018.03.161>
- [2] X. Zhou, T. Korenaga, T. Takahashi, T. Moriwake, S. Shinoda, A Process monitoring controlling system for the treatment of wastewater containing chromium (VI), *Water Res.*, 27 (1993) 1049-1054. [https://doi.org/10.1016/0043-1354\(93\)90069-T](https://doi.org/10.1016/0043-1354(93)90069-T)
- [3] Y. Pang, Zeng, G.M. Zeng, L. Tang, Y. Zhang, Y. Y. Liu, X.X. Lei, M.S. Wu, Z. Li, C. Liu, Cr(VI) reduction by *Pseudomonas aeruginosa* immobilized in a polyvinyl alcohol/sodium alginate matrix containing multi-walled carbon nanotubes, *Bioresour. Technol.*, 102

- (2011) 10733-10736. <https://doi.org/10.1016/j.biortech.2011.08.078>
- [4] D. Mohan, C.U. Pittman, Activated carbons and low cost adsorbents for remediation of tri- and hexavalent chromium from water, *J. Hazard. Mater.*, 137 (2006) 762-811. <https://doi.org/10.1016/j.jhazmat.2006.06.060>
- [5] X. Guo, X. Lü, The need for biofuels in the context of energy consumption, *Advances in 2nd generation of bioethanol production*, Woodhead Publishing Series in Energy, CRC press, New York, pp 9-30, 2021. <https://doi.org/10.1016/B978-0-12-818862-0.00004-2>
- [6] W. Zheng, K. Phoungthong, F. Lü, L.M. Shao, P.J. He, Evaluation of a classification method for biodegradable solid wastes using anaerobic degradation parameters, *Waste Manage.*, 33 (2013) 2632–2640. <https://doi.org/10.1016/j.wasman.2013.08.015>
- [7] I.G. Coronilla, L. M. Barrera, E. C. Urbina, Kinetic, isotherm and thermodynamic studies of amaranth dye biosorption from aqueous solution onto water hyacinth leaves, *J. Environ. Manage.*, 152 (2015) 99-108. <https://doi.org/10.1016/j.jenvman.2015.01.026>
- [8] A. Zhang, X. Li, J. Xing, G. Xu, Adsorption of potentially toxic elements in water by modified biochar: A review, *J. Environ. Chem. Eng.*, 8 (2020) 104196. <https://doi.org/10.1016/j.jece.2020.104196>
- [9] U. Upadhyay, I. Sreedhar, S.A. Singh, C.M. Patel, K. L. Anitha, Recent advances in heavy metal removal by chitosan based adsorbents, *Carbohydr. Polym.*, 251(2021) 117000. <https://doi.org/10.1016/j.carbpol.2020.117000>
- [10] E. Guibal, Interactions of metal ions with chitosan-based sorbents: A review, *Sep. Purif. Technol.*, 38 (2004) 43-74. <https://doi.org/10.1016/j.seppur.2003.10.004>
- [11] W.C. Chong, J.F. Chin, Z.W. Heng, H.C. Teoh, Y.L. Pang, Recent development of magnetic biochar crosslinked chitosan on heavy metal removal from wastewater - Modification, application and mechanism, *Chemosphere*, 291 (2022)133035. <https://doi.org/10.1016/j.chemosphere.2021.133035>
- [12] J. Cheng, F. Xiao, W. Cao, C. Yang, J. Chen, Z. Luo, Removal of heavy metals from aqueous solution using chitosan-combined magnetic biochars, *J. Colloid Interface Sci.*, 540 (2019) 579-584. <https://doi.org/10.1016/j.jcis.2019.01.068>
- [13] A. Choudhary, A. Kadawasara, S.S Poonia, P. kumar, V.K. Janu, Pyrolytic preparation of active carbons from peanut shell biomass for adsorptive elimination of fluoride from groundwater of Shekhawati region, *Orient. J. Chem.*, 38 (2022) 1338-1350. <http://dx.doi.org/10.13005/ojc/380602>
- [14] APHA, Standard methods for the examination of water and wastewater. 21st edition, american public health association/American water works wssociation/water environment federation, Washington DC, 1288 pages, 2005. www.apha.org
- [15] M. Thompson, SLR. Ellison, R. Wood, Harmonized guidelines for single-laboratory validation of methods of analysis (IUPAC Technical Report). *Pure Appl. Chem.*, 74 (2002) 835–855. <https://doi.org/10.1351/pac200274050835>
- [16] I. Langmuir, The constitution and fundamental properties of solids and liquids, *J. Am. Chem. Soc.*, 183 (1917) 102–105. <https://doi.org/10.1021/ja02268a002>
- [17] H. Freundlich, Über die adsorption in lösungen, *Zeitschrift für Physikalische Chem.*, 57 A (1907) 385–470. <https://doi.org/10.1515/zpch-1907-5723>
- [18] S. Ahmed and S. Ikram, Chitosan and its derivatives: A Review in recent innovations, *Int. J. Pharm. Res.*, 6 (2015) 14-30. [http://dx.doi.org/10.13040/IJPSR.0975-8232.6\(1\).14-30](http://dx.doi.org/10.13040/IJPSR.0975-8232.6(1).14-30)
- [19] Y. S. Ho, G. McKay, The kinetics of sorption of divalent metal ions onto sphagnum moss peat, *Water Res.*, 34 (2000) 735–742. [https://doi.org/10.1016/S0043-1354\(99\)00232-8](https://doi.org/10.1016/S0043-1354(99)00232-8)
- [20] S. Lagergren, On the theory of the so-called adsorption of dissolved substances, solubility (Theoretical chemistry), *Sven. Vetenskapskad. Handlingar*, 24 (1898) 1–39. <https://cir.nii.ac.jp/crid/1570009750361875328>
- [21] X. Duan, D. Wang, G. Qian, J.C. Walmsley, A. Holmen, D. Chen, X. Zhou, Fabrication of K-promoted iron/carbon nanotubes composite catalysts for the Fischer–Tropsch synthesis of lower olefins, *J. Energy Chem.*, 22 (2016) 13-20. <https://doi.org/10.1016/j.jechem.2016.01.003>
- [22] J. Deng, Y. Liu, S. Liu, G. Zeng, X. Tan, B. Huang, X. Tang, S. Wang, Q. Hua, Z. Yan, Competitive adsorption of Pb(II), Cd(II) and Cu(II) onto chitosan-pyromellitic dianhydride modified biochar, *J. Colloid. Interface. Sci.*, 506 (2017) 355-364. <https://doi.org/10.1016/j.jcis.2017.07.069>
- [23] R. Li, W. Liang, H. Huang, S. Jiang, D. Guo, M. Li, Z. Zhang, A. Ali, J.J. Wang, Removal of

- cadmium (II) cations from an aqueous solution with aminothiourea chitosan strengthened magnetic biochar, *J. Appl. Polym. Sci.*, 135 (2018) 46239. <https://doi.org/10.1002/app.46239>
- [24] W. Zhang, S. Mao, H. Chen, L. Huang, R. Qiu, Pb(II) and Cr(VI) sorption by biochars pyrolyzed from the municipal wastewater sludge under different heating conditions, *Bioresour. Technol.*, 147 (2013) 545–552. <https://doi.org/10.1016/j.biortech.2013.08.082>
- [25] F. Golbabaei, Z. Sadeghi, A. Vahid, A. Rashidi, On-line micro column preconcentration system based on amino bimodal mesoporous silica nanoparticles as a novel adsorbent for removal and speciation of chromium (III, VI), *J. Environ. Health Sc. Eng.*, 13 (2015) 1-12. <https://doi.org/10.1186/s40201-015-0205-z>
- [26] M.M. Eskandari, B. Kalantari, Dispersive liquid-liquid microextraction based on task-specific ionic liquids for determination and speciation of chromium in human blood, *J. Anal. Chem.*, 70 (2015) 1448-1455. <https://doi.org/10.1134/S1061934815120072>
- [27] H. Shirkhanloo, M. Ghazaghi, M.M. Eskandari, Cloud point assisted dispersive ionic liquid-liquid microextraction for chromium speciation in human blood samples based on isopropyl 2-[(isopropoxycarbothioly) disulfanyl], *Anal. Chem. Res.*, 10 (2016)18-27. <https://doi.org/10.1016/j.ancr.2016.10.002>
- [28] H. Shirkhanloo, M. Ghazaghi, H.Z. Mousavi, Chromium speciation in human blood samples based on acetyl cysteine by dispersive liquid-liquid biomicroextraction and in-vitro evaluation of acetyl cysteine/cysteine, *J. Pharm. Biomed. Anal.*, 118 (2016) 1-8. <http://dx.doi.org/10.1016/j.jpba.2015.10.018>
- [29] S. A. H. Mirzahosseini, the evaluation and determination of heavy metals pollution in edible vegetables, water and soil in the south of Tehran province by GIS, *Arch. Environ. Prot.*, 41 (2015) 63-72. <https://doi.org/10.1515/aep-2015-0020>
- [30] M Arjomandi, A review: analytical methods for heavy metals determination in environment and human samples, *Anal. Methods Environ. Chem. J.*, 2 (2019) 97-126. <https://doi.org/10.24200/amecj.v2.i03.73>
- [31] V. Leitea, B. Jesisa, V. Duartea, V. Constantinob, C. Izumic, J. Trontoa, F. Pintoa, Determination of chromium (VI) by dispersive solid-phase extraction using dissolvable Zn-Al layered double hydroxide intercalated with L-Alanine as adsorbent, *Microchem. J.*, 146 (2019) 650–657. <https://doi.org/10.1016/j.microc.2019.01.063>
- [32] A. Lace, D. Rayan, M. Bowkett, J. Cleary, Chromium Monitoring in water by colorimetry using optimised 1,5-diphenylcarbazide method, *Int. J. Environ. Res. Public Health*, 16 (2019) 1803; <https://doi.org/10.3390/ijerph16101803>